CORE
Metadata, citation and similar papers at core.ac.uk
Provided by NASA Technical Reports Server

Spatially and Temporally Resolved Measurements of Velocity in a H_2-air Combustion-heated Supersonic jet

Daniel Bivolaru[*], and Andrew D. Cutler[†],
The George Washington University, Newport News, VA 23602

and

Paul M. Danehy[‡], Richard L. Gaffney, Jr[§], and Robert A. Baurle[**]
NASA Langley Research Center, Hampton VA, 23681-2199

This paper presents simultaneous measurements at multiple points of two orthogonal components of flow velocity using a single-shot interferometric Rayleigh scattering (IRS) technique. The measurements are performed on a large-scale Mach 1.6 (Mach 5.5 enthalpy) H_2-air combustion jet during the 2007 test campaign in the Direct Connect Supersonic Combustion Test facility at NASA Langley Research Center. The measurements are performed simultaneously with CARS (Coherent Anti-stokes Raman Spectroscopy) using a combined CARS-IRS instrument with a common path 9-nanosecond pulsed, injection-seeded, 532-nm Nd:YAG laser probe pulse. The paper summarizes the measurements of velocities along the core of the vitiated air flow as well as two radial profiles. The average velocity measurement near the centerline at the closest point from the nozzle exit compares favorably with the CFD calculations using the VULCAN code. Further downstream, the measured axial velocity shows overall higher values than predicted with a trend of convergence at further distances. Larger discrepancies are shown in the radial profiles.

Nomenclature

d	=	exit diameter of jet
x	=	x-coordinate, along jet centerline
y	=	y-coordinate, perpendicular to the jet centerline
u	=	axial velocity, in the x-axis direction
v	=	radial velocity, in the y-axis direction
$\bar{u}$	=	mean axial velocity
$\bar{v}$	=	mean radial velocity
u'	=	$u - \bar{u}$
v'	=	$v - \bar{v}$
x_0	=	0, x-origin defined at the nozzle exit plane
y_0	=	0, y-origin at the jet centerline
$\boldsymbol{k}_0$	=	incident wave vector of the probe laser
$\boldsymbol{k}_{s1}$	=	scattered light wave vector in a first direction to measure the v-component of velocity
$\boldsymbol{k}_{s2}$	=	scattered light wave vector anti parallel with $\boldsymbol{k}_{s1}$ to measure the u-component of velocity

[*] Research Scientist, The George Washington University/MAE, NASA LaRC/ASOMB, MS 493, AIAA Senior Member
[†] Professor, The George Washington University/MAE, 100 Old Oyster Point Road, Suite 200, AIAA Associate Fellow
[‡] Research Scientist, Advanced Sensing and Optical Measurement Branch, MS 493, AIAA Associate Fellow
[§] Aerospace Engineer, Hypersonic Air-breathing Propulsion Branch, MS 168, AIAA Senior Member
[**] Aerospace Engineer, Hypersonic Air-breathing Propulsion Branch, MS 168, AIAA Associate Fellow

I. Introduction

BOTH experimental and computational fluid dynamics (CFD) methods are widely used in the design and analysis of hypersonic air-breathing engine flow paths. Most CFD methods employ models that are based on statistical properties of flow turbulence. The actual statistical properties can be known only when multiple flow properties are measured simultaneously, and when the spatial scales (hundreds of microns or less) and temporal scales (hundreds of nanoseconds or less) of the turbulent fluctuations are resolved. Correlations between those properties lead to a more detailed understanding of complex flow behavior and aid in the development of multi-parameter turbulence models for computational fluid dynamics codes.[1,2]

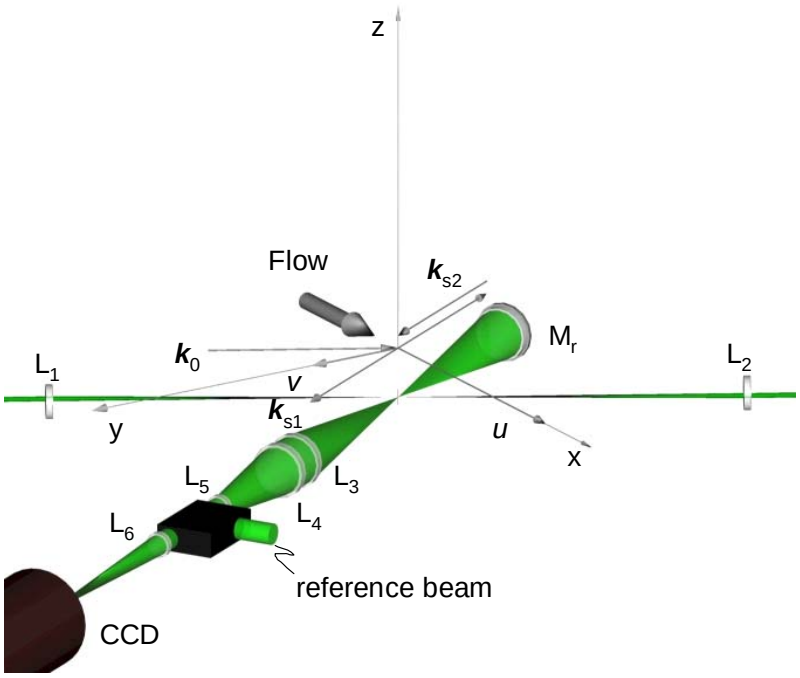

Figure 1. Measurement configuration (all vectors are in the horizontal plane)

This paper presents simultaneous measurements at multiple points of two orthogonal components of flow velocity using an interferometric Rayleigh scattering (IRS) technique.[3] The measurements are performed simultaneously with a combined CARS-IRS (Coherent Anti-stokes Raman Spectroscopy – Interferometric Rayleigh Scattering) instrument that uses the same 9-nanosecond pulsed, injection seeded, Nd:YAG laser beam (at 532 nm) for both techniques.[4] The experiments were conducted at NASA Langley Research Center's Direct Connect Supersonic Combustor Test Facility (DCSCTF) on an axisymmetric Mach 1.6 H_2-air combustion-heated jet flow at enthalpy levels of a Mach 5.5 hypersonic flight.[5,6,7] A complementary paper describes in detail the measurements of flow temperature obtained simultaneously with velocities using the CARS system.[8]

II. Description of the Instrument

Figure 1 shows a schematic of the experimental setup for IRS. The IRS instrument measures by directing and focusing polarized light from a green beam laser (wave vector $\boldsymbol{k}_0$) using a first lens (L_1) to a measurement volume within the gas medium, providing laser illumination from one direction as shown in the figure. Laser light, elastically scattered in the measurement volume by the gas molecules, is collected from two opposite directions using a lens (L_3) for one direction and a mirror (M_r) for the other. Both collected signal beams ($\boldsymbol{k}_{s1}$ and $\boldsymbol{k}_{s2}$), directly collected by the lens L_3 and collected and retroreflected toward the lens by the mirror M_r, are combined in a single signal beam. This collected scattered light (the signal) is then collimated by lenses L_4 and L_5, combined with a fraction of the main laser light (reference beam) using a beam combiner/mixer, and passed through a solid etalon for spectral analysis (black box). The interference fringe pattern generated at the output of the etalon (by the lens L_6) is recorded by a CCD camera at 20 Hz, the laser pulse and the measurement repetition rate. The resulting recorded image, as shown in **Fig. 2**, contains the scattered light spectral information in two horizontal patterns, and the laser frequency (concentric ring pattern) used as

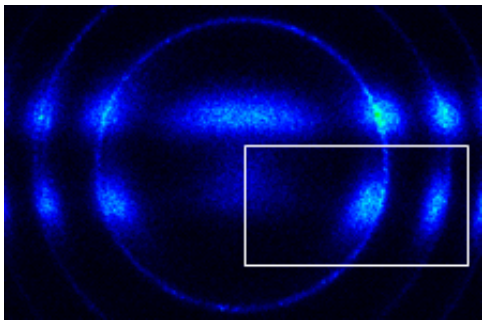

Figure 2. Single-shot interferogram containing reference laser frequency (concentric ring pattern) and Rayleigh scattered light spectral information (horizontal patterns). The interferogram is obtained in the axi-symmetric supersonic jet, with the top horizontal pattern for the radial component, and the bottom horizontal pattern for the axial component of velocity.

a reference frequency. The horizontal patterns are the images of the laser beams (viewed from two directions) filtered out spectrally by the etalon.

Each horizontal pattern determines an independent velocity component. In-house developed image processing software extracts spatial and spectral information for both velocity components from each interferogram image. These data are fit with theoretical Rayleigh scattering models (Gaussian functions) to determine the Doppler shift frequency of the spectra with respect to the reference laser frequency. The magnitude of each flow velocity component is then calculated from the Doppler shift.

An example of spatially and temporally resolved IRS spectra from two closely separated measurement locations is shown in **Fig. 3**. The temporal resolution is about 40 ns,[3] and the spatial distance between spectra is about 0.4 mm. Figure 3(a) and Fig. 3(b), show the experimental data (black symbols), the theoretical best fit (black line), and the residual between them (blue). The fit functions are Gaussian functions (red lines) with the narrow peak (the reference frequency) being at the laser frequency. Figure 3(b) shows spectra with the reference peaks at the noise level that are predominant in the measurements presented here.

The bisector of the angle formed by the incident laser beam and the viewing direction gives the direction of the velocity component being measured. Since the collection directions of the scattered light are anti-parallel, the two components of velocity being measured are orthogonal. An angle of 60±1° (forward scattering) was used to measure the streamwise component of velocity, *u*, and an angle of 120±1° (backward scattering) to measure the component of velocity in a perpendicular direction, *v*.

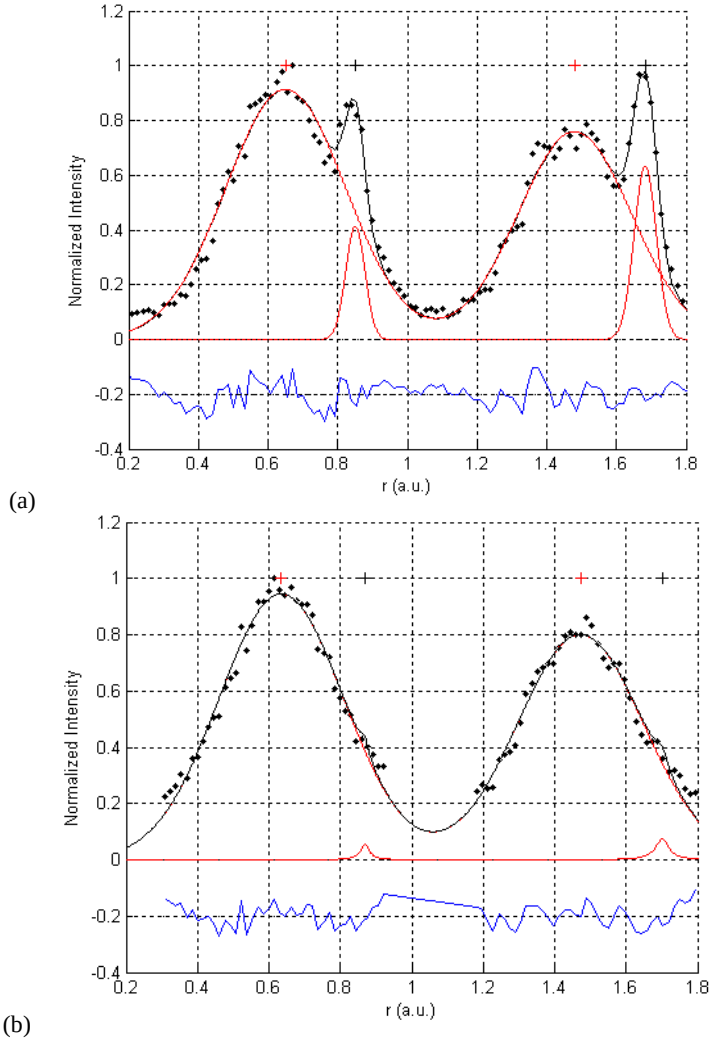

Figure 3. Single-shot IRS spectra from two spatial locations as shown in the inset of Fig. 2. (a), mixed spectra of signal and reference laser of equal amplitude, and (b), combined spectra with the reference intensity at the noise level. The plot shows the experimental data (black symbols), the theoretical best fit (black line), and the residual between them (blue). The fit functions of the signal and the reference are marked in red: the narrower peaks are at the laser reference frequency. The spatial width between spectra is about 0.4 mm.

The volume imaged by the IRS system contains four non-evenly spaced measurement points of about 0.2 mm^3 each in the images of the laser beams (Fig. 2). These points are distributed along about 1.6 mm of the laser beam at its focus. The inner points of this pattern are situated about 0.8 mm apart, with at the next points being about 0.4 mm further apart on each side. More detailed information about the IRS system and data analysis can be found in references 9 and 10.

III. Facility Description

The nozzle assembly installed in the DCSCTF consists of a water-cooled nickel flange, a water-cooled copper nozzle block, and a stainless steel cone.[5] The convergent-divergent nozzle is formed within the copper block, and its contour was designed by the method of characteristics to provide a uniform Mach 1.6 flow at the exit. A coflow nozzle is formed by the space between the copper block and the steel cone. The coflow nozzle is connected to the

fuel supply (H_2) but it is not used during the experiment reported herein. The nozzle is instrumented with thermocouples and pressure taps.

In the facility, the nozzle assembly is fixed horizontally, so the laser beam delivery system and the IRS optics translate horizontally in two dimensions to probe multiple spatial locations in a horizontal plane. Two linear translation stages were used as means of translating the system up to 0.6 m in the cross flow directions, and 1 m in the streamwise direction (~9 to 16 nozzle diameters). The translation stages have a position accuracy of 200 μm and repeatability of ±12 μm. Due to physical and equipment constraints (including constraints imposed by the CARS system) two arrangements were used to probe the flow. The *upstream* setup permitted measurements from 0.87 to 7 nozzle diameters downstream of the nozzle exit plane, while the *downstream* setup allowed measurements between 6 and 13 nozzle diameters. Overlapping test points were set at the intersection of these two regions to check reproducibility of the measurements. All measurement points were performed in a horizontal semi-plane passing through the centerline of the jet (and containing the laser beams). The jet was captured by an exhaust pipe (to minimize the fire hazard during experiments) placed axially in front of the jet for both the upstream and the downstream tests at about 24 nozzle diameters downstream of the nozzle exit. The pipe, with an inside diameter of 24.8 cm, is connected to a vacuum sphere (22 meters in diameter) and is the lowest cross-sectional area in the exhaust system. The pressure in the sphere was reduced to a few torr (mm Hg) before runs, and the typical increase in pressure during a 50 sec run was of the order of 140 torr. Other details of the experimental setup in the facility, including the jet nozzle and combustor design, can be found in references 4 and 6. **Figure 4** shows an infrared image (in the range of 3 μm to 5 μm) of the jet flow during the facility run at Mach 5.5 enthalpy. The image shows the shock-free jet flow with some larger turbulent flow structures towards the downstream end of the field of view (flow from left to right). The curved objects in the field of view are the nozzle assembly on the left and silhouettes of the opto-mechanical components of the measurement system.

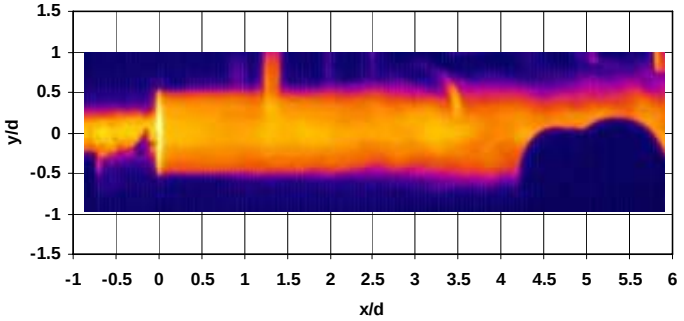

Figure 4. Infrared image of the jet during the facility run at Mach 5.5. The flow is from left to right. The curved objects in the field of view are optical components.

IV. The Velocity Distribution

A. CFD simulations using the VULCAN code

For the present work, the jet into ambient air was simulated numerically using the VULCAN CFD code. This code solves the Navier-Stokes equations using a finite volume discretization. The inviscid fluxes were computed using the low dissipation flux split scheme of Edwards in conjunction with a 3rd order MUSCL stencil and a limiter by Van Leer. Thermodynamic properties for the thermally perfect gases were computed using the curve fits of McBride et. al. The turbulence was modeled using the k-omega model of Wilcox. The computational domain extended 60 jet diameters downstream of the nozzle exit and 40 jet diameters radially from the centerline to the outer boundary. It also included the facility combustor downstream of the fuel injectors and the Mach 1.6 nozzle. Calculations were made with both coarse (124,556 points) and fine grids (494,332 points) to ensure that the solutions were grid resolved. The combustor conditions[††] were at a total pressure of 419 kPa and a total

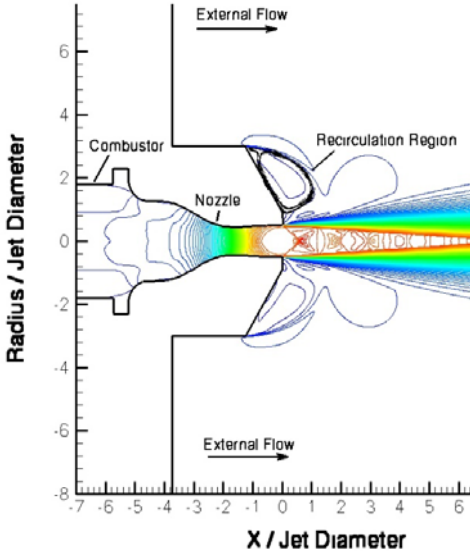

Figure 5. Mach number contours lines in the combustor, nozzle and the upstream flow. The colors in the order, red, yellow, green, and blue, show contour lines of decreasing Mach number.

[††] Initial calculations used conditions published by Cutler[5] (P_0 = 419 kPa and T_0 = 1327 K) however, these did not match the CARS temperature data.[8] A second set of calculations was then made at P_0 = 419 kPa and a total temperature of 1397 K.

temperature of 1397 K. In the surrounding ambient air the total pressure was 1 atmosphere with a 20 m/sec velocity imposed to mimic the airflow in the test cell and to aid numerical convergence. **Figure 5** shows Mach contours in the flow near the jet exit. A shear layer develops between the high velocity jet flow and the very low velocity ambient airflow. At these conditions the pressure in the jet exit is slightly higher than the ambient pressure resulting in weak waves reflecting back and forth between the shear layer and the centerline.

The flow through the exhaust pipe into the vacuum sphere generated choked flow at the entrance or somewhere in the pipe. This close proximity of the exhaust pipe to the nozzle exit affected the downstream free jet properties slightly. Two CFD calculations were performed to investigate this effect, one without the pipe and a second with the pipe. In the simulation neglecting the exhaust pipe, the jet centerline became subsonic about 11 jet diameters from the nozzle exit and continued to decelerate further downstream. With the pipe, the flow downstream of the sonic point (at about Mach 0.8) re-accelerates to a supersonic Mach number. The exhaust pipe influences the downstream subsonic flow and slightly affects the upstream core flow (about 0.5% of the main stream velocity).

B. Streamwise Velocity Profiles near the Centerline of the Jet

Figure 6 shows the average axial velocity u_{ave} ($\bar{u}$) as function of the normalized distance from the nozzle exit plane, *x*/d (where the nozzle exit plane is at *x*/d = 0 ± 0.02, and d = 6.35 cm), at *y*/d = 0.04 ± 0.06 near the centerline. The centerline distribution of the average radial velocity v_{ave} ($\bar{v}$) is plotted similarly in the same figure using open symbols. The data plot is divided into two parts: upstream (black symbols) and downstream (red symbols), corresponding to the two distinctive sets of measurements that were performed. Error bars of one standard deviation about the mean velocity are shown in the figure. Due to the experiment modifications from the upstream to downstream measurements (it is possible that the measurement locations are not overlapped) there is a jump in the average velocity of about 50 m/sec (one standard deviation at that location) at the intersection of these two datasets. Slightly different flow conditions in the combustor might also have a contribution to this jump.[8] A plot of the standard deviation of the measured velocity versus the normalized distance from the nozzle plane is also shown in the lower part of the figure.

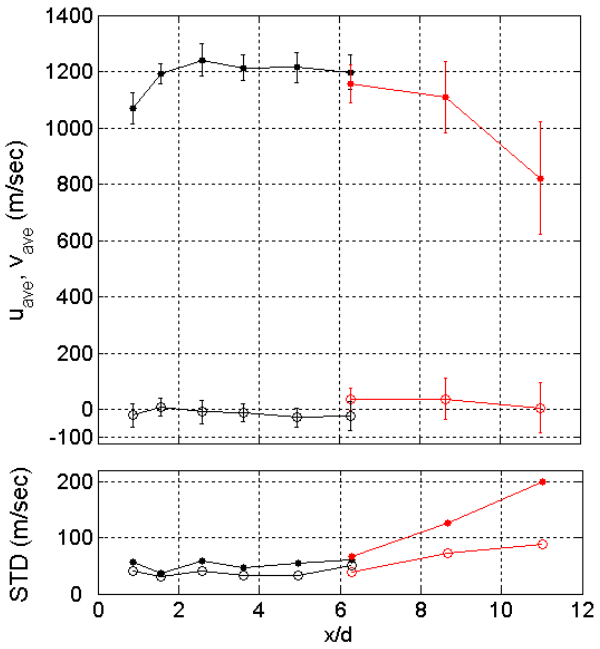

Figure 6. Near centerline average velocity *u* and *v* (top), and the standard deviation of the measured velocity (bottom) as function of the normalized distance *x*/d from the nozzle exit plane.

The systematic errors of the instrument cannot be fully quantified (at this time) for the entire range of the instrument. The measurements in stagnant air show that the error of measuring zero velocity in the axial direction has a systematic error of about 20 m/sec. The uncertainty in the scattering angle of ±1°, relative to the velocity vector being measured, contributes to a systematic error in calculating the velocity of about ±1.5% or about ±15 m/sec. Therefore, the total systematic error in the velocity measurements quantifiable at this time becomes about 25 m/sec. The instrument's random error in the facility, based on the ability to determine the free spectral range of the interferogram,[9,10] is found to be about 30 m/sec for the axial component and about 4.5 m/sec for the radial component of velocity. The errors associated with the change in the bias velocity as a function of velocity and gas temperature are unknown, although in Reference 11 it was determined for a similar setup that the velocity bias was no more than 30 m/sec over the range of temperatures used in this experiment. The instrument systematic error of measuring zero velocity (20 m/s) was subtracted from the dataset measured values to correct this known error.

As expected, the flow turbulence, as measured by the standard deviation in the velocity measurements, significantly increases with the distance from the nozzle exit. Increases are as much as about 7 times and 3 times the near-field velocity fluctuations of *u* and *v*, respectively.

The centerline measurement results are summarized in **Table 1** as a function of the normalized distance x/d along with the average of the measured velocity, $\bar{u}$ and $\bar{v}$, the standard deviation of the measurement, σ_u and σ_v, and the number of measurements, N_u and N_v, used to compute the velocity average from about 200 measurements per set point. The reported velocity measurements are the average from two spatially separated measurement locations about 0.4 mm apart. The effective measurement volume is thus about 0.2 × 0.2 × 0.6 mm. Each mean velocity data point presented here is obtained from one run performed at that location. On average, about 5 times more data is available at one location. All this data will be processed and reported in the near future.

x/d	$\bar{u}$ (m/sec)	σ_u (m/sec)	$\bar{v}$ (m/sec)	σ_v (m/sec)	N_u	N_v
0.87	1069	57	-21	40	141	29
1.58	1192	36	8	30	82	80
2.6	1241	59	-9	40	94	95
3.6	1213	46	-11	32	81	82
4.9	1214	54	-28	33	93	89
6.3	1197	61	-23	50	77	71
6.3	1156	66	38	39	102	107
8.9	1110	125	38	73	93	92
11.0	821	200	6	89	58	64

Table 1. The axial velocity data near the centerline of the jet (at y/d = 0.04 ± 0.006 where d = 6.35 cm). Red indicates downstream data.

The first data point in Fig. 6, the closest to the nozzle exit, compares favorably with CFD calculations.[3,7] Further downstream the measured velocity shows overall higher values than the free jet CFD simulation, but both fall, as one would expect, in the downstream region of the jet. This is shown again in **Fig. 7** for single-shot measurements. The data is obtained simultaneously from two spatial points at the specified *x*/d locations (red and black symbols) and from a rapid scan along the jet performed continuously between 0.87 and 4.9 nozzle diameters downstream (red and black circle symbols). For comparison, the CFD is computed on the centerline (light blue) and off axis at *y*/d = 0.1 (dark blue). The comparison of the measurements with the CFD data at *y*/d = 0.1 suggests a possible off axis measurement (in the expansion flow regions), although this cannot explain the ~200 m/s discrepancy.

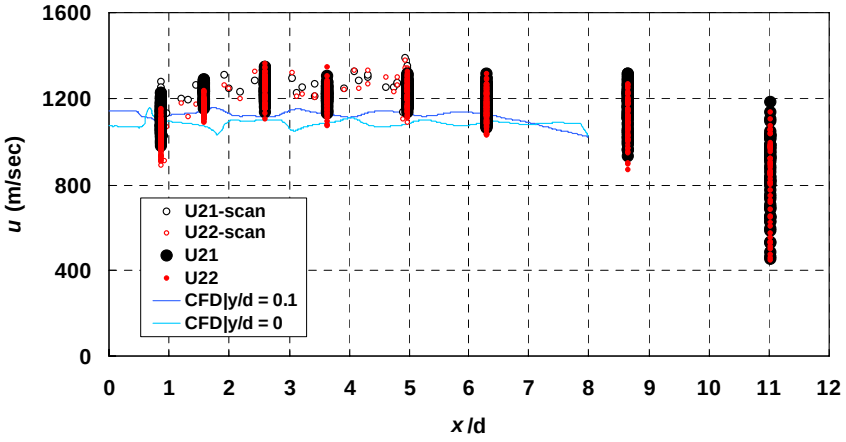

Figure 7. Single-shot measurements and CFD calculations of the axial velocity as function of the normalized distance x/d from the nozzle exit plane. CFD data computed on the centerline (turquoise) and off axis at y/d = 0.1 (blue).

Figure 6 shows a sudden change in *v* between the upstream and downstream regions. An explanation is that the bisector of the angle formed by the direction of the laser beam and the receiving optics which define the direction of the measurement does not perfectly overlap the direction of the velocity vector intended to be measured, i.e., the resultant wave vector is not parallel with the velocity vector. The contribution of the *v* velocity component to the measured velocity *u* is negligibly small, but the contribution of the *u* component (at about 1100 m/sec) to the measured *v* component (less than 100 m/sec) can be significant. The induced measurement error in the *v*-component can be as much as 20 m/sec per degree of offset angle. This error is unavoidable when the measurement of this angle cannot be obtained with accuracy better than ±1°, though it can be minimized by a calibration of the instrument. For the presented data set, such laborious calibration was not possible before every run in the test facility due to a multitude of factors including the setup configuration and the time constraint. For the upstream measurements the offset angle is about +3°, and is unknown for the downstream measurements.

Measurements performed at four points simultaneously are shown in **Fig. 8** for the axial velocity component as a function of time. The measurements are obtained near the jet centerline at x/d = 0.87, the closest location to the nozzle exit plane (first point in Fig. 6, Fig. 7, and in Table 1). Again, for the current configuration, the four non-evenly spaced points are distributed symmetric along about 1.6 mm of the laser beam at its focus (as shown in the horizontal pattern of Fig. 2). The furthest two inner points around the center of pattern are situated about 0.8 mm apart (between u_1 and u_3), with the closest (the sides of the pattern) at about 0.4 mm apart (between u_1 and u_2 or u_3 and u_4). The red trace shows clearly a difference in the velocity measured between points at this location visible also at locations up to 2.6 nozzle diameters downstream as shown in Fig. 7.

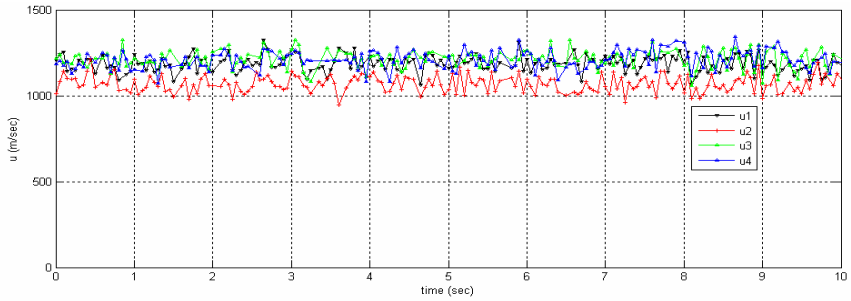

Figure 8. Simultaneous measurement of the axial velocity at four spatial locations near the jet centerline of a Mach 1.6/Mach 5.5 enthalpy jet: The measurements are obtained near the jet exit at x/d = 0.87.

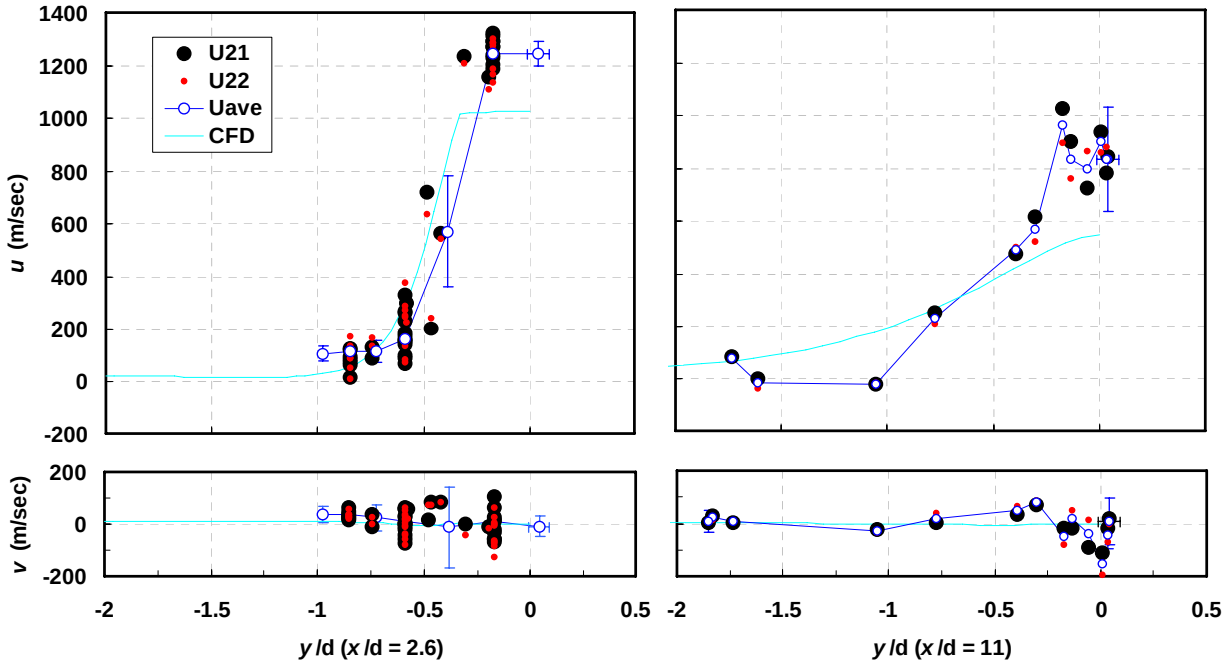

(a) (b)

Figure 9. Radial profiles of velocity at two axial locations in the flow. (a), velocity profiles obtained at x/d = 2.6 in the upstream, and (b), at x/d = 11 in the downstream. The blue curves indicate the CFD solutions of an ideal free jet at Mach 1.6 (Mach 5.5 enthalpy).

C. Radial Profiles

Figure 9 shows two measured radial profiles and the CFD calculations of the axial (u) and radial (v) velocity at two axial locations: 2.6 and 11 nozzle diameters downstream. The red and black symbols represent single shot data from rapid scans of the flow in the radial direction. These data are obtained simultaneously from measurements at two spatially separated measurement locations about 0.4 mm apart. The data marked in dark blue with error bars were obtained from averaging multiple single-shot measurements. Similarly, the data without error bars are obtained by averaging the measurements from two spatial locations. It is clear that for the profile at x/d = 2.6 (Fig. 9(a)) the

axial velocity does not reach zero at or around one nozzle diameter outside jet, as predicted in the CFD solution (light blue line). (Note in Figure 5 that the CFD solution has a recirculation region attached to the outer shroud that slows the flow at this location.) In the downstream portion of the jet, a velocity profile[12] approximating a Gaussian distribution, should be reached as shown by the CFD calculation, but an approximate "top hat" profile is shown by the instantaneous measured data instead (Fig. 9(b)). This may indicate that the jet in the CFD solution is diffusing faster than what is seen in the data. Outside the shear layer at $x/d = 2.6$, the radial velocity component (v) is three times higher than the predicted one. However, the 20 m/s far-field velocity was assumed as a boundary condition in the CFD calculation and is not a true prediction of far-field properties. Also at these axial locations a difference between calculated and experimental maximum velocity u of about 200 m/sec exists in the jet.

These discrepancies cannot be explained entirely at this time and no conclusions should be drawn, though careful analysis was performed on both the Rayleigh spectra processing and the CFD modeling. A variety of factors can lead to such discrepancies: First, not every property was measured so some assumptions were made in setting CFD boundary conditions. For example, the current CFD solutions were made with an assumed inflow turbulence level. Previous work has shown[7] that the diffusion rate of the jet is sensitive to turbulence levels at the nozzle exit. Lower turbulence levels lead to a longer core flow while higher turbulence levels lead to more rapid diffusion and Gaussian-like profiles. Further processing of the data may reveal lower actual turbulence levels than what was assumed for the CFD calculations. Similarly, the nozzle exit pressure and the local near-field external pressure (expected to be slightly lower than atmospheric) were not measured so that the exact jet pressure ratio was not known. This pressure ratio affects the expansion/compression wave structure in the jet. It is also possible that the low pressure at the suction pipe entrance has the effect of accelerating the jet significantly near the exhaust pipe. Therefore the velocity u must be higher and in regions of subsonic flow the acceleration will reduce the jet diameter (by conservation of mass) as shown by the measurements including at the edge of the boundary; A simple back of the envelope calculation employing Euler's equation suggests that this increase is very small (~5 m/sec) and can not explain the large discrepancy in the core (~200 m/sec) versus the small discrepancy at the edge (~100 m/sec). Second, unknown measurement errors while moving the probe volume, such as a variable reference intensity that could offset velocity with a variable quantity (unlikely); and Third, the most of concern, the unknown influence of Hydrogen combustion products and the Raman vibrational excitation of species (from CARS) on the Rayleigh spectra and its distribution of velocities.

D. Two-Point, and Axial-Radial Velocity Correlations

Figure 10 demonstrates spatial correlations of velocities measured simultaneously at two closely separated spatial points. The distance between points used to measure u_1 and u_2 (or v_1 and v_2) is 0.4 mm. The markers in red indicate upstream data at x/d = 0.87, and the markers in black, the downstream data at x/d = 11.02. Both measurements of u and v show correlation, i.e., the data are scattered along a line with the slope of approximately 45°. This indicates that a large fraction of the turbulence scale is resolved at least down to about 0.4 mm or about 6/1000 of a nozzle diameter for this type of flow.

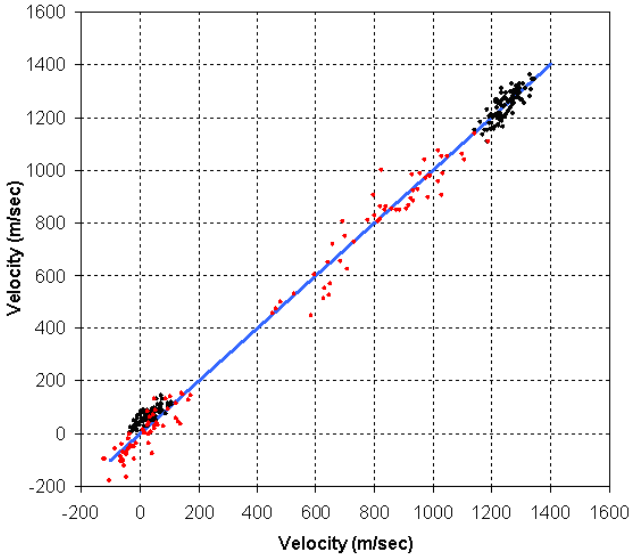

Figure 10. Two-point correlations of velocities. The distance between points is 0.4 mm. Black and Red markers indicate upstream and the downstream data at x/d = 0.87 and x/d = 11, respectively.

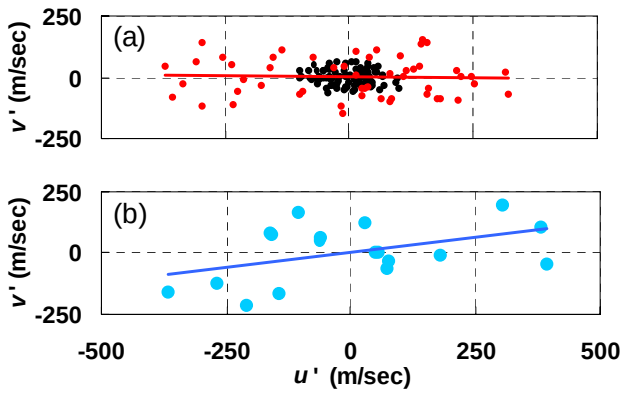

Figure 11. Correlation of velocities in the jet flow. (a), near the centerline at (*x*, *y*)/d = (2.6, 0.04) in the upstream (black), and at (*x*, *y*)/d = (11, 0.04) in the downstream. (b), velocity correlations in the mixing layer at (*x*, *y*)/d = (2.6, -0.4).

The correlations between $u' = u - \bar{u}$ and $v' = v - \bar{v}$ velocities, where u and v are the velocity components measured simultaneously, and $\bar{u}$ and $\bar{v}$ are the corresponding mean velocities, are shown in **Fig. 11**. The black and red markers in Fig. 11(a) show the scatter in the data near the centerline at x/d = 2.6, and in the downstream at x/d = 11, respectively. In Fig. 11(b), the graph shows the velocity data obtained in the mixing layer at (x, y)/d = (2.6, -0.4). The velocities have a relatively low correlation near the jet axis both in the upstream ($\overline{u'^2}$ = 2214 m^2/sec^2, $\overline{v'^2}$ = 958 m^2/sec^2, $\overline{u'v'}$ = -136 m^2/sec^2) and in the downstream flow ($\overline{u'^2}$ = 34335 m^2/sec^2, $\overline{v'^2}$ = 6108 m^2/sec^2, $\overline{u'v'}$ = -571 m^2/sec^2), as is expected based on the axisymmetry of the flowfield. In the mixing layer the velocities are correlated ($\overline{u'^2}$ = 43754 m^2/sec^2, $\overline{v'^2}$ = 12650 m^2/sec^2, $\overline{u'v'}$ = 10359 m^2/sec^2) as expected in a turbulent shear layer; note that in this data set v' is positive radially inward and thus the sign of $\overline{u'v'}$ is consistent with expectations for a turbulent shear layer. Furthermore, turbulent energy and other statistical parameters necessary for turbulent model development can be extracted from this dataset. For example, the square root of the turbulent kinetic energy $\sqrt{\frac{1}{2}\left(\overline{u'^2} + \overline{v'^2} + \overline{w'^2}\right)}$, where v' is approximately w' for axisymmetric flow, is measured to be 3.7% in the upstream at x/d = 2.6, about 18.5% in the downstream at x/d =11, and 32% in the mixing layer at (x, y)/d = (2.6, -0.4).

v. Conclusions

Measurements of two-components of flow velocity have been obtained at multiple points using a single-shot interferometric Rayleigh scattering (IRS) technique for the first time in a large-scale combustion flow. The measurements are performed on a Mach 1.6, Mach 5.5 sensible enthalpy, H_2-air combustion heated jet at NASA Langley Research Center. The measurements are simultaneous with CARS using a combined CARS-IRS instrument that uses the same 9-nanosecond pulsed, injection seeded, Nd:YAG laser beam (at 532 nm) as the probe laser.

The data presented here summarizes preliminary measurements of the radial and streamwise velocity components near the centerline of the jet and at two radial profiles of streamwise velocity for the mixing case. The first data point of the test matrix, the closest to the nozzle exit, compares favorably with the CFD calculations using the VULCAN code. Further downstream the measured velocity shows overall higher values than the CFD values with a trend of convergence further downstream. Radial velocities are small in the mean, relative to the fluctuations, while discrepancies between the mean radial velocity and the CFD values are greater than expected. A variety of factors can cause such discrepancies such as the assumptions made in setting the CFD boundary conditions, unknown measurement errors while moving the probe volume, noisy Rayleigh spectra and the difficulty of fitting such noisy spectra. Of the most concern, is the unknown influence of Hydrogen combustion products and the Raman vibrational excitation of species (from CARS) on the Rayleigh spectra and its distribution of velocities.

The instrument precision and its systematic errors in the facility were estimated for the axial component to be about 30 m/sec, and 25 m/sec, respectively. For the radial component the instrument precision is better than 5 m/sec except that errors in alignment of the measurement coordinate system with the jet coordinate system can lead to larger systematic errors in v. The contribution of the u-component (at about 1100 m/sec) to the measured v-component (typically less than 100 m/sec) for a small angular misalignment can be as much as 20 m/sec per degree. The systematic error in velocity u is negligibly small in such a case.

Finally, the instrument resolved the turbulent time and length scales of the jet flow, as shown in the comparison of turbulent properties and computations, proving it to be a valuable tool in combustion diagnostics and in supporting CFD modeling. Plausible measurements of the turbulent kinetic energy, $\overline{u'v'}$, the main component of the turbulent Reynolds stress, were presented.

Acknowledgment

We like to acknowledge numerous colleagues contributing to this work in one way or another: Diego Capriotti, James Downey, Rachel Johnson, Stephen Jones, Mark Kulick, Barry Lawhorne and his team, Brian Luoto, Joseph Lee, Gaetano Magnotti, Tom Mills, Peter Parker, Lloyd Wilson, Markus Weikl, and especially Sarah Tedder. We also acknowledge Phil Drummond and both management teams of HAPB and ASOMB at NASA/LaRC for supporting and patience during these prolonged experiments.

This work was supported by the NASA Fundamental Aeronautics Program – Hypersonics Project, Experimental Capabilities and Propulsion Disciplines and Mr. George Rumford, program manager of the Defense Test Resource Management Center (DTRMC) Test and Evaluation/Science and Technology (T&E/S&T) program, under the Hypersonic Test focus area.

References

1 J. Philip Drummond, Paul M. Danehy, Daniel Bivolaru, Richard L. Gaffney, Sarah A. Tedder, and Andrew D. Cutler, "Supersonic combustion research at NASA, 2007 Fall Technical Meeting," Eastern States Section of the Combustion Institute, University of Virginia, October 21-24, 2007.

2 R. A., Baurle, "Modeling of High Speed Reacting Flows: Established Practices and Future Challenges," AIAA-2004-0267, 42th Aerospace Sciences Meeting, Reno, NV, January 5-8, 2004.

3 Bivolaru, D., Danehy, P. M., Gaffney, Jr. R. L., and Cutler, A. D., "Direct-View Multi-Point Two-Component Interferometric Rayleigh Scattering Velocimeter," AIAA-2008-0236, 46th Aerospace Sciences Meeting, Reno, NV, January 9-12, 2008.

4 D. Bivolaru, P. M. Danehy, K. D. Grinstead, Jr., S. Tedder, A. D. Cutler, "Simultaneous CARS and Interferometric Rayleigh Scattering" AIAA AMT-GT Technology Conference, San Francisco, AIAA-2006-2968 June (2006).

5 A. D. Cutler, G. Magnotti, R. Baurle , D. Bivolaru , S. Tedder , P. M. Danehy, M.C. Weikl, F. Beyrau, and T. Seeger, "Development of Supersonic Combustion Experiments for CFD Modeling", AIAA Paper 2007-0978, 45th AIAA Aerospace Sciences Meeting and Exhibit, Reno, Nevada , January 8-11 (2007).

6 Danehy, P. M., Magnotti, G., Bivolaru, D., Tedder, S., and Cutler, A. D., "Simultaneous Temperature and Velocity Measurements in a Large-Scale, Supersonic, Heated Jet," JANNAF2008, Massachusetts, May, 2008

7 Gaffney Richard L., Jr., "Numerical Simulation of a Co-Axial Supersonic-Combusting free-jet Experiment," JANNAF2008, Massachusetts, May, 2008

8 S. Tedder, P. M. Danehy, G. Magnotti and A. D. Cutler, "CARS Temperature Measurements in a Combustion-Heated Mach 1.6 Jet," AIAA-2009-0524, 47th AIAA Aerospace Sciences Meeting, Orlando, FL, January, 2009.

9 D. Bivolaru, P. M. Danehy, R. L. Gaffney, Jr. and A. D. Cutler, "Direct-View Multi-Point Two-Component Interferometric Rayleigh Scattering Velocimeter," 46th AIAA Aerospace Sciences Meeting and Exhibit 7 - 10 January 2008, Reno, Nevada, AIAA Paper 2008-236

10 D. Bivolaru, P. M. Danehy, A. D. Cutler, "Multipoint Inteferometric Rayleigh Scattering using Light Recirculation," Paper Number 2008-3708, 26th AIAA Aerodynamic Measurement Technology and Ground Testing Conference, Seattle, WA June 23-26, 2008

11 S. Tedder, D. Bivolaru, P. M. Danehy, M.C. Weikl, F. Beyrau, T. Seeger, A. D. Cutler "Characterization of a Combined CARS and Interferometric Rayleigh Scattering System", AIAA Paper 2007-0871, 45th AIAA Aerospace Sciences Meeting and Exhibit, Reno, Nevada, January 8-11 2007.

12 Yuceil, K. B., Otugen, M. V.," Scaling Parameters for Underexpanded Supersonic Jets," Physics of Fluids, Vol. 14, Nr. 12, December 2002.